Two-Dimensional Finite-Element Analysis of Pinning-Induced Stress in HTS Power Transmission Cables Made of 2G Superconducting Tapes With and Without Magnetic Substrate

Muzaffer Erdogan, Şükrü Yildiz, Ahmet Cicek, and Fedai Inanir

***Abstract*—In a two-layer superconducting cable, we numerically investigated the effect of magnetic properties and alignment of the substrates of the tapes on the stress distribution induced by a very high transported electric current. The calculations are carried out for two tapes, with one being on top of the other. Sharp peaks of induced stress very close to the edges of the tapes are observed. When nonmagnetic substrates are used, the stress distributions on the tapes are almost identical, as well as being much lower than those in the cases involving ferromagnetic (FM) substrates. When the tapes are arranged face to face with FM substrates on the outer sides, the stress distribution arisen in the outer tape is considerably higher than that in the inner tape. In contrast, flipping both layers, so that the tapes are back to back, gives rise to a much lower stress over the outer tape than that over the inner tape.**

***Index Terms*—Finite-element method (FEM), magnetic substrate, stress distribution, superconducting tapes, superconducting wires.**

I. Introduction

HIGH-CURRENT superconducting (SC) cables combine many parallel coated conductors with current-carrying capabilities larger than 250 $A \cdot cm^{-1}$ in self-field at 77 K [1]. In such cables, the tapes can be wound spirally around a central former [2], [3]. In cables consisting of more than one tape, each tape is exposed not only to its self-field but also to the combined magnetic field from other tapes [4]. Since SC cables work under very high self-magnetic fields created by the transport current, they are always subject to very high magnetic forces, which can result in internal stress in the cable, being strongly related to the distribution of the current and magnetic flux [5]–[8]. High internal stress levels may lead to performance degradation of the cables. In order to ensure a secure cable operation, it is necessary to predict their magnetoelastic behaviors such as internal stress or strain.

For almost two decades, numerous works have been dedicated to investigating magnetoelastic effects generated by the flux pinning in superconductors under magnetic field. In order to explain the giant magnetostriction on the order of 10^{-6} measured on the SC BSCCO, the first model was developed by Ikuta *et al.* [9] based on the flux-pinning-induced stress. Later, the magnetoelastic problem was theoretically solved within the critical state model for different SC geometries, such as slab, stripe, disk, etc., under electromagnetic forces [10]–[13]. In addition, various flux line dynamic effects on stress and strain resulting from the pinning-induced forces have been extensively studied [14]–[17]. Considerable attention has been paid on the fracture behaviors resulting from the pinning-induced force in the SC slab and cylinder geometries employing the linear elastic fracture theory [18], [19]. Mints and Brandt [20] and Gao *et al.* [21] examined the crack inclusion and collinear crack problems in superconductors. Consequently, these studies deal typically with theoretical calculations of the flux-pinning-induced stress and strain distributions or cracking behavior in different SC geometries under parallel or perpendicular magnetic field. However, Inanir and Erdogan proposed a model calculation for strain in an SC specimen in the presence of transport current [22]. Yong and Zhou calculated the stress and magnetostriction induced by flux pinning for a flat SC strip of a type-II superconductor subject to a transport current [23]. Jing *et al.* proposed a theoretical model to analyze the transverse normal stress and interfacial shearing stress induced by the electromagnetic force in the SC coated conductor in increasing and decreasing transport current [24].

To the best of our knowledge, there is a lack of information on the pinning-induced stress due to the Lorentz force created by the interaction of the transport current and self-magnetic field in multilayer SC power transmission cables carrying transport current. In SC devices, internal stress induced by Lorentz force occurs when they are subject to a transport current or an external magnetic field. They may be vulnerable to internal deformation, such as microcracks, which degrade both the mechanical and electromagnetic characteristics of superconductors.

Manuscript received December 10, 2015; revised February 7, 2016; accepted February 25, 2016. Date of publication March 28, 2016; date of current version May 13, 2016. This work was supported by the Scientific and Technological Research Council of Turkey (TUBITAK) under Grant 110T876. This paper was recommended by Editor L. Chiesa.

M. Erdogan is with the Department of Physics, Namik Kemal University, Tekirdag 59030, Turkey (e-mail: merdogan@nku.edu.tr).

Ş. Yildiz is with the Department of Metallurgical and Materials Engineering, Ahi Evran University, Kirşehir 40000, Turkey.

A. Cicek is with the Department of Electrical Engineering, Jack Baskin School of Engineering, University of California at Santa Cruz, Santa Cruz, CA 95064 USA.

F. Inanir is with the Department of Physics, Yildiz Technical University, Istanbul 34349, Turkey.

Color versions of one or more of the figures in this paper are available online at http://ieeexplore.ieee.org.

Digital Object Identifier 10.1109/TASC.2016.2544827

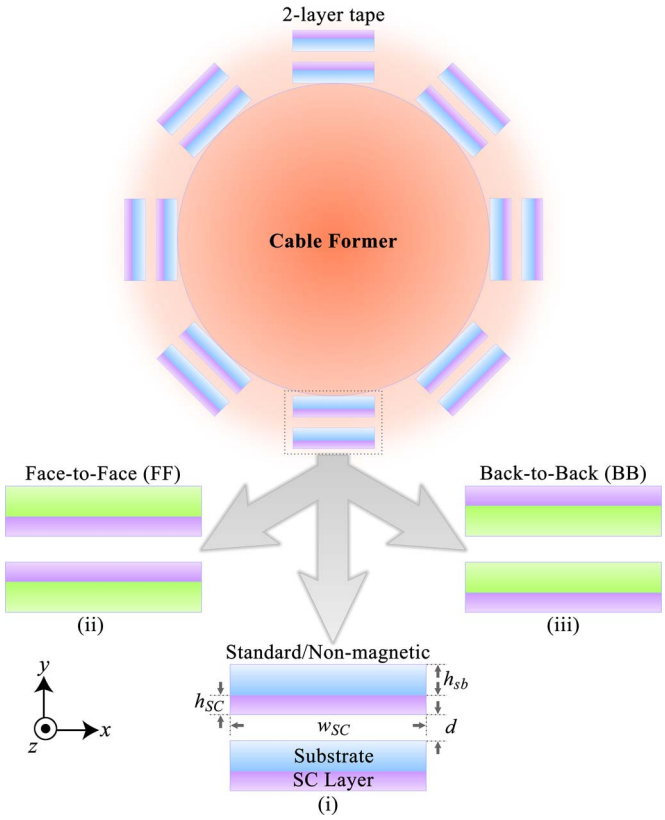

Fig. 1. Three different cable designs proposed in the calculations: (i) nonmagnetic substrate; (ii) face to face (FF), in which the SC tapes face each other; and (iii) back to back (BB), such that the FM substrates face each other. Elements are not drawn to scale for clarity.

In this paper, we study the stress behaviors of two-layer second-generation (2G) high-T_c SC (HTS) power transmission cables consisting of coated SC tapes with or without a ferromagnetic (FM) substrate through finite-element method (FEM) simulations. The calculations are restricted to the constant critical current density and constant permeability for the SC layer and FM substrate, respectively.

II. Modeling

The two-layer HTS SC cable model employed in numerical modeling, which is composed of multiple HTS coated superconductor tapes with a rectangular cross section is depicted in Fig. 1. The tapes lie along the z-axis, and the transport current flows in this direction.

The magnetic field is taken to be uniform in the z-direction; therefore, the current density, electrical field, and the magnetic vector potential have no x- or y-components. FEM simulations are performed with COMSOL Multiphysics software via the ac/dc module, in which Maxwell equations are implemented successfully in the $A-V$ formulation, the name referring to the electromagnetic potentials used as state variables. In the $A-V$ formulation, the governing equation for the dynamical analysis is given by Ampere's Law

$$\nabla \times \left(\frac{1}{\mu_r \mu_0} \nabla \times \vec{A} \right) = \vec{j} \tag{1}$$

TABLE I
Chosen Geometrical and Physical Parameters for HTS Cables and in the Implementation of FEM Simulations

Quantity (Unit)	Description	Value
I_c (A)	The critical current per SC tape	100
α	winding pitch	∞
E_c (V/m)	Electric field criterion	$1\text{x}10^{-4}$
B_0	Critical current density parameter	0.36
β	Critical current density parameter	1.2
μ_r	Relative permeability of FM substrates	500
w_{sc} (mm)	Width of a SC tape	4
h_{sc} (μm)	Height of a SC tape	2
w_{sb} (mm)	Width of FM substrate	4.2
h_{sb} (μm)	Height of FM substrate	80
R_i (mm)	Radius of the inner layer	19.95
R_o (mm)	Radius of the outer layer	20.93
d (μm)	Distance between two layers	980
R_{CD} (mm)	Radius of the computational domain	~25xR_o
N	Number of SC tapes in each layer	17
f (s^{-1})	Frequency of applied current	50

with

$$\vec{E} = -\frac{\partial \vec{A}}{\partial t} - \nabla V \tag{2}$$

where μ_r is the relative magnetic permeability; μ_0 is the magnetic permeability of vacuum; $\vec{A}$ is the magnetic vector potential along the z-axis; $\vec{j}$ is the overall current density; and ∇V represents the potential difference per unit length of tape along the z-direction, which is uniform across the tape cross section. The total magnetic vector potential A is composed of the contributions from the self-magnetic field and external magnetic field generated by the current in the surrounding conducting tapes. It can be expressed in the integral form as [25], [26]

$$A = \sum_{i=1}^{N} \frac{\mu_0 I}{8\pi w_{\mathrm{SC}} h_{\mathrm{SC}}} \int_S \ln(r)\, dS \tag{3}$$

where N is the number of tapes in a layer, I is the current flowing in tapes, and r is the distance from the source. All parameters used in FEM simulations are listed in Table I. The integration is taken over the complete cross section of the tapes. The vector potential expression given by (3) is established as the boundary of computational domain [25]. The employed boundary condition (BC) can be defined by using the "magnetic potential" BC in the ac/dc module of COMSOL, thus ascertaining the vector potential at the outer boundary of the model depicted in Fig. 2. The characteristics of the current density in the SC part is governed by [27], [28]

$$j_s = j_c \tanh\left(\frac{E}{E_c}\right) \tag{4}$$

where j_s is the current density in the SC tape, j_c is the critical current density, E is the electric field, and E_c is the electric field criterion (e.g., 1 μV/cm). Since the electromagnetic problem involves discrete rotational symmetry due to the geometry of the cable, FEM simulations are conducted by considering only two tapes in Fig. 1, with one on top of another.

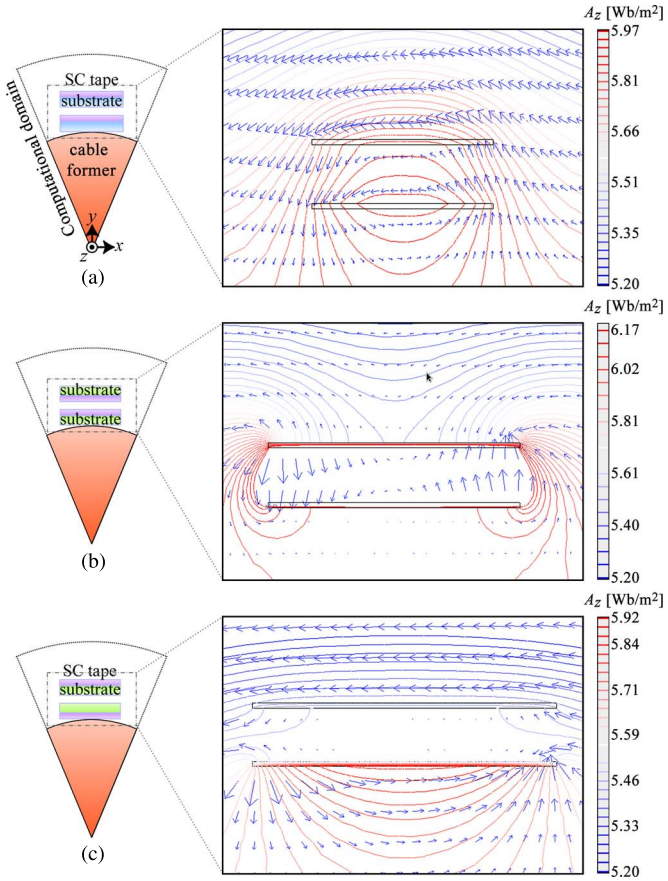

Fig. 2. Calculated magnetic vector potential and magnetic field distributions around the two SC tape layers for $I_a = 75$ A, in computational domains, depicted on the left of each plot, comprising a $2\pi/N$ angular section of the cable, for the (a) nonmagnetic, (b) FF, and (c) BB cases. The arrows represent the magnetic field, whereas contours of the magnetic vector potential are color coded on the right of each plot.

The SC layer and substrate are considered to be isotropic and elastic. The basic equations for evaluating the stress in the coated conducting tapes under transport current were already derived by Jing *et al.* [24]. The stress distribution inside the SC layers is calculated following similar procedures to those given in [24] and [29], which may be summarized as follows. The Lorentz force density $\vec{f} = \mu_0 \vec{J} \times \vec{B}$ acting on an SC tape and the interfacial shearing stress $q(x)$ between the substrate and the SC tape satisfy the equations [24]

$$\frac{1}{\overline{E}_{\rm sc} h_{\rm sc}} \int_{-w_{\rm sc}/2}^{x} [q(\xi) + f(\xi)]\, d\xi - \frac{2}{\pi \overline{E}_{\rm sb}} \int_{-w_{\rm sc}/2}^{\frac{w_{\rm sc}}{2}} \frac{q(\xi)}{\xi - x} d\xi = 0 \tag{5}$$

$$\int_{-w_{\rm sc}/2}^{\frac{w_{\rm sc}}{2}} q(\xi) d\xi = 0 \tag{6}$$

where x is the distance from the edge of the SC tape, satisfying $-w_{\rm sc}/2 < x < w_{\rm sc}/2$; $\overline{E}_{\rm sc} = E_{\rm sc}/(1-\nu_{\rm sc}^2)$; $\overline{E}_{\rm sb} = E_{\rm sb}/(1-\nu_{\rm sb}^2)$; E is the Young modulus; and ν is Poisson's ratio. The subscripts sc and sb stand for the SC tape and the FM substrate, respectively.

After appropriate transformations, (5) and (6) can be rewritten in the form

$$\int_{-1}^{r} \left[(1-t^2)^{-\frac{1}{2}} + h\left(\frac{t w_{\rm sc}}{2}\right) \right] dt - 2c\Gamma(r) = 0 \tag{7}$$

$$\int_{-1}^{1} (1-t^2)^{-\frac{1}{2}} \Gamma(r) dr = 0 \tag{8}$$

with the following definitions:

$$\Gamma(r) = \frac{\pi g(r)}{\mu_0 J_c^2 h_{\rm sc}^2},\ q\left(\frac{x w_{\rm sc}}{2}\right) = p(x),\ c = 4\frac{h_{\rm sc}}{w_{\rm sc}} \frac{E_{\rm sc}}{E_{\rm sb}} \frac{1-\nu_{\rm sb}^2}{1-\nu_{\rm sc}^2}.$$

The solution to the integral equation (7) is of the form $p(r) = (1-t^2)^{-1/2} g(r)$ [24]. The constant c has a strong influence on the stress distribution, which, in turn, depends on the stiffness of the SC tape and FM substrate. The transverse normal stress distribution in the SC tape is given by [24]

$$\frac{\sigma(r)}{\sigma_0} = \int_{-1}^{r} \left[(1-t^2)^{-\frac{1}{2}} \Gamma(r) + h\left(\frac{t w_{\rm sc}}{2}\right) \right] dt \tag{9}$$

where

$$\sigma_0 = \frac{\mu_0 J_c^2 h_{\rm sc}^2}{\pi E_{\rm sc}}. \tag{10}$$

We took the Young modulus of the SC tape as $\overline{E}_{\rm sc} = 50$, which is large enough so that the normal stress distribution for the SC tape is consistent with that of the FM substrate.

In all figures, three configurations are illustrated in the following order: (i) nonmagnetic substrate; (ii) FF, in which the SC tapes with FM substrates face each other; and (iii) BB, such that the FM substrates face each other.

III. Results and Discussion

The calculated magnetic vector potential and magnetic field distributions around the two SC tape layers in the computational domain, which are depicted on the left of each plot, comprising a $2\pi/N$ angular section of the cable, are shown in Fig. 2 for the instant current value $I_a = 75$ A. The figure reveals the following qualitative observations: 1) in the FF configuration [see Fig. 2(b)], the self-magnetic fields created by the inner and the outer SC layers are in the same direction and stronger normal field components occur at the edges of the conductors, whereas 2) in the BB configuration [see Fig. 2(c)], they are in opposite directions; therefore, the FM substrates between the two SC layers experience a smaller resultant field. In this case, the stress distributions on the SC tapes are lower than that in the FF configuration.

Fig. 3 depicts 1-D stress distribution for the nonmagnetic case [case (i) in Fig. 1], which is induced on a single SC tape in the outer layer for different amplitudes of the applied current. We only show the outer one on the layer since the behavior of the inner layer is similar. We apply an ac current of 75-A amplitude. After passing through the maximum current magnitude of 75 A, an outward (negative) electromagnetic stress occurs

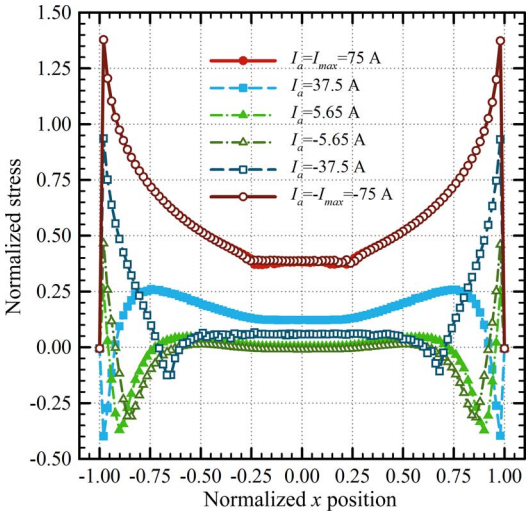

Fig. 3. Widthwise normalized stress distribution of the SC tapes with nonmagnetic substrate ($\mu_r = 1$) for intermediate values of the applied current of 75-A amplitude.

at the edges of the SC tapes. Moreover, the stress becomes maximum in the proximity of the edges and then decreases monotonically toward the center of the sample, around which it is almost constant.

We attribute the existence of the maximized stress at the edges to the influence of the magnetic fields generated by the neighboring SC tapes and to the demagnetization effect due to the present geometry, as indicated in Fig. 2(a). Lorentz force $\vec{f} = \mu_0 \vec{J} \times \vec{B}$ becomes maximum in the region close to the surface area due to the penetration of the vortices into the conductor in this region. The reason for the plateau of the stress near the center of the sample is the cancelation of the forces generated by the two vortices penetrating from the right and left edges of the sample.

It is also shown in Fig. 3 that the stress throughout the sample falls down sharply as the intermediate current value decreases and that at least two kinds of stresses act on the sample. For instance, when the current decreases down to $I_a = 37.5$ A, a negative stress occurs at the edges of the sample, while a positive stress occurs at the central region. This is attributed solely to the direction of the induced current in the negative z-direction. While most of the cross section of the sample is acted by a positive stress, a small section close to the edges experiences negative stress. When the current is reduced to $I_{\max}/2$, the stress is halved, as well. The difference between the stress distributions in the cases $I_a = 37.5$ A and $I_a = -37.5$ A arises from the fact that they are in the second (decreasing) and in the third (increasing) quadrants in a cycle of the applied current. Although the two current values have the same magnitude, different regimes lead to different current distributions [22]. The two distinct peaks in the sample for very low current values are also related to the current distribution in the sample. The same stress distributions are observed for the extreme values $I_a = \pm 75$ A, as expected. The behavior of the stress distribution computed in the SC tape with nonmagnetic substrate is in agreement with the case of a coated SC [24]. This ensures the validity of the computational model, in terms of the simulation strategy.

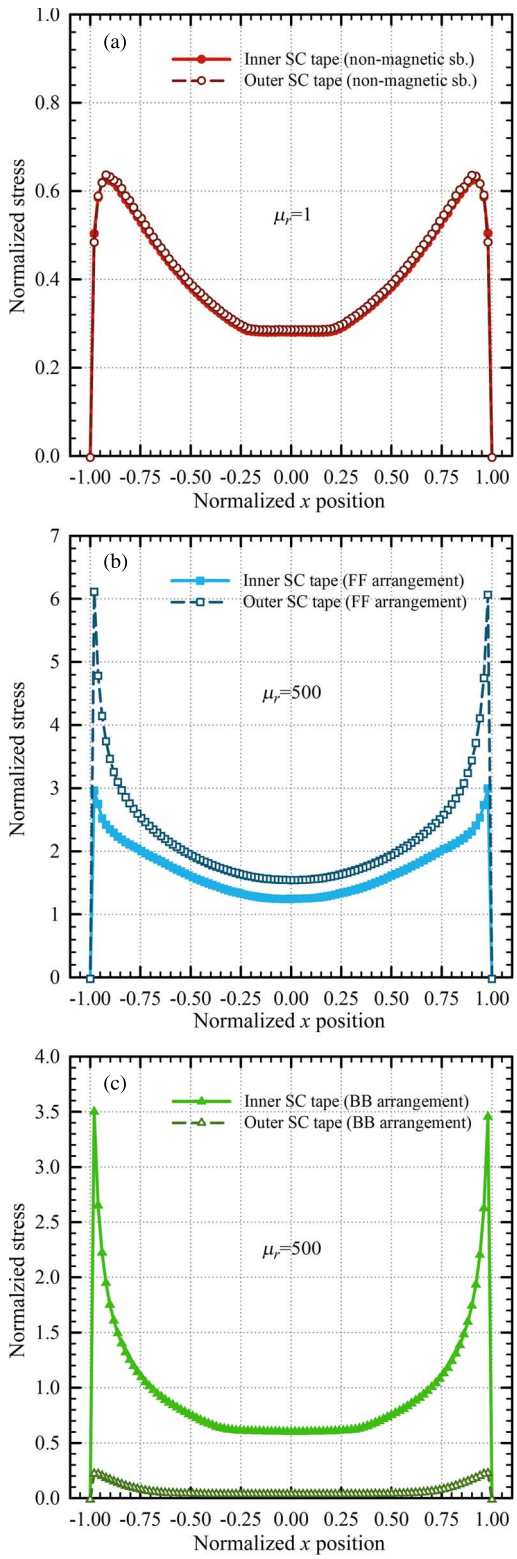

Fig. 4. Widthwise stress distributions on the SC tapes for the three cases; (a) with a nonmagnetic substrate ($\mu_r = 1$)), (b) with an FM substrate ($\mu_r = 500$) in FF arrangement, and (c) with an FM substrate in BB arrangement. Here, the stress is normalized by $\sigma_0 = \mu_0 J_c^2 h_{\rm sc}^2/\pi E_{\rm sc}$. The calculations are for only $I_{\max} = 75$ A.

The stress distribution in both inner and outer SC tapes is shown in Fig. 4(a), where a nonmagnetic substrate [case (i) in Fig. 1] is employed, when the applied current amplitude is

$I_a = 75$ A. As observed in Fig. 4(a), the stress distributions are very close in the two layers. Note that the stress increases abruptly from the sample center toward the edges.

Fig. 4(b) compares the two stress distributions occurring in the inner and the outer SC tapes for the FF configuration [case (ii) in Fig. 1] with an FM substrate for which $\mu_r = 500$. Here, we see that the stress in the outer tape is considerably higher than that in the inner tape, unlike the case in Fig. 4(a). The reason for the observed effect is stronger localization of the magnetic field, particularly at the edges of the SC tapes. This excess field causes penetration of a larger current into the SC layer, yielding a larger structural force.

The stress distributions for the BB configuration are shown in Fig. 4(c), where the stress in the outer SC tape is significantly lower than that in the inner one. This is because the perpendicular component of the self-magnetic field experienced by the outer tape is smaller than that in the inner tape. Note that the inner SC tape is subject to minimum structural stress in this case.

Current density distributions on the SC tapes for all configurations are illustrated in Fig. 5. The curves correspond to the current density distributions along the widthwise center line of the SC tapes, while the insets show the cross-sectional distributions. In Fig. 6, the calculated Lorentz force distributions for all configurations are shown. Comparing the figures, we may deduce that, 1) in the FF configuration, high current density [see Fig. 5(b)] together with a high normal magnetic field component at the edges [see Fig. 2(b)] cause the accumulation of the Lorentz force at these regions, particularly on the outer SC tape, as shown in Fig. 6(b). 2) The resemblance of the current [see Fig. 5(c)] and the force density [see Fig. 6(c)] distributions on the outermost surface of the outer SC tape in the BB configuration is attributed to the uniform and parallel magnetic field to this surface, as shown in Fig. 2(c). The peaks in the force density distribution at the edges of the inner SC tape are because of the high normal component of the magnetic field here, as indicated in Fig. 2(c).

We observe in Fig. 6 that, 1) in the FF arrangement [see Fig. 6(b)], the force density distribution has peaks at the edges of the inner and outer SC tapes, which is consistent with Fig. 4(b); 2) in the BB arrangement [see Fig. 6(c)], the force density accumulates on the outermost surface of the outer SC tape, while it has peaks at the edges of the inner SC tape.

IV. Conclusion

The stress analysis of an HTS two-layer power transmission cable employing 2G SC tapes is numerically investigated within a 2-D computational scheme via FEM simulations through the COMSOL Multiphysics software. Although the calculations are performed for the values given in Table I, the following qualitative conclusions are assumed to hold true for different values of the parameters, such as N, I_a/I_c, R_i, R_o, due to the rotational symmetry of the computational domain, while quantitatively different results are expected. In this paper, stress distributions of three cases are considered: (i) nonmagnetic substrate; (ii) FF, in which the SC tapes face each other; and (iii) BB, in which the FM substrates face each other.

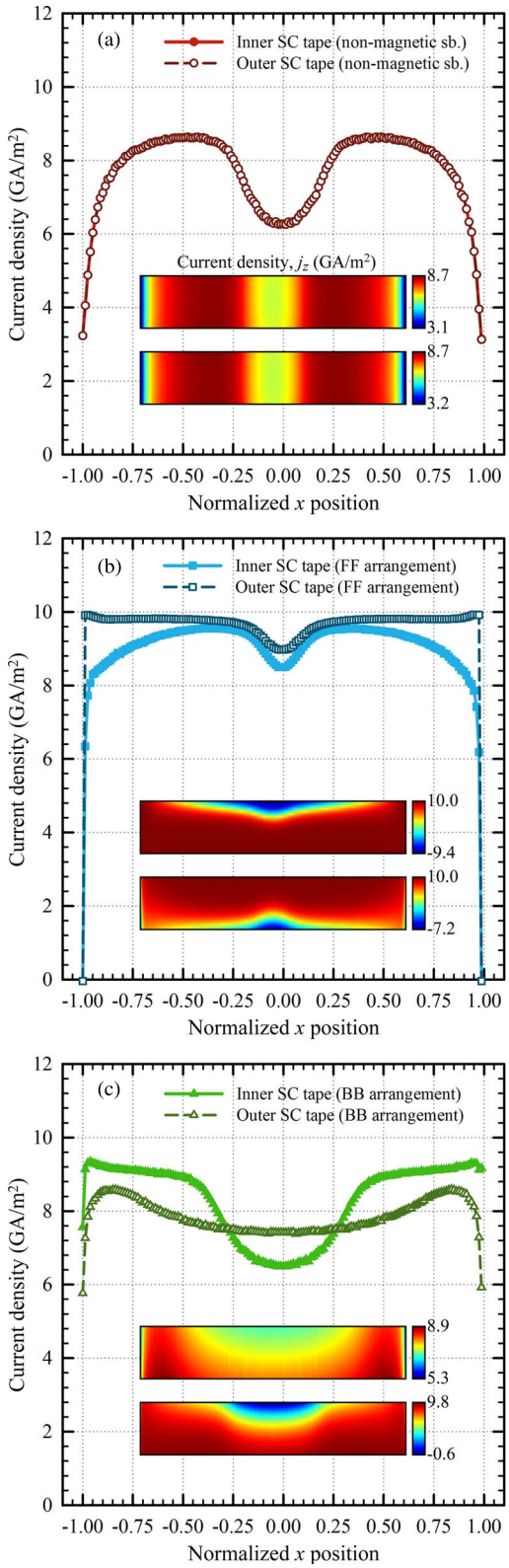

Fig. 5. Current density distributions on the SC tapes for (a) a nonmagnetic substrate, (b) the FF arrangement, and (c) the BB arrangement. Insets, which are not drawn to scale for clarity, show the distributions of the current density on cross sections.

Our findings may be summarized as follows:

1) In all cases, sharp peaks of the stress distribution very close to the edges of the SC tapes are observed, indicating

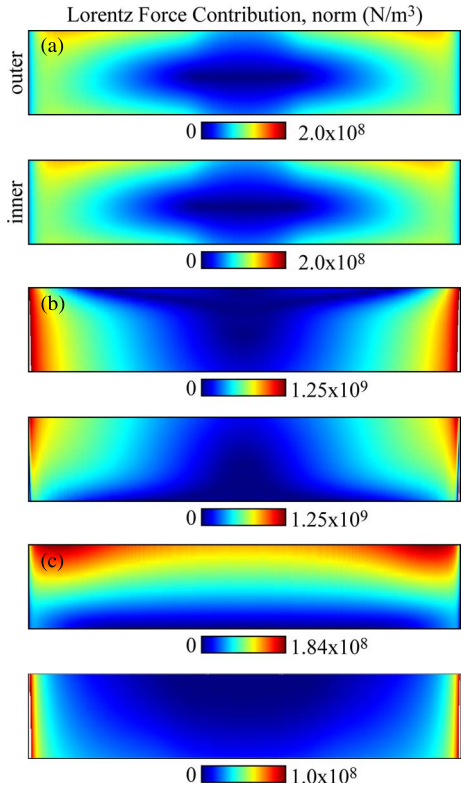

Fig. 6. Lorentz force density distributions acting on the two SC tapes for (a) a nonmagnetic substrate, (b) the FF arrangement, and (c) the BB arrangement. Dimensions are not drawn to scale for clarity.

an elevated risk of fracture following the application of a current.

2) For a nonmagnetic substrate, the stress distributions on the two SC tapes are almost equal at every point.
3) The stress occurring in the tapes with nonmagnetic substrates is much lower than in the tapes with FM substrates with $\mu_r = 500$, except for the outer tape in the BB configuration.
4) For the FF arrangement with an FM substrate, the stress distribution arisen in the outer tape is considerably higher than that in the inner tape.
5) For the BB arrangement, on the other hand, the stress distribution in the inner tape is much higher than that in the outer tape.

REFERENCES

[1] D. W. Hazelton, F. Roy, and P. Brownsey, "Recent developments in 2G HTS coil technology," presented at the European Conf. Applied Superconductivity, Den Haag, The Netherlands, 2011, Paper 1-LB-07.
[2] M. Takayasu, L. Chiesa, L. Bromberg, and J. V. Minervini, "Cabling method for high current conductors made of HTS tapes," *IEEE Trans. Appl. Supercond.*, vol. 21, no. 3, pp. 2340–2344, Jun. 2011.
[3] D. C. van der Laan, X. F. Lu, and L. F. Goodrich, "Compact $GdBa_2Cu_3O_{7-\delta}$ coated conductor cables for electric power transmission and magnet applications," *Supercond. Sci. Technol.*, vol. 24, no. 4, Apr. 2011, Art. no. 042001.
[4] J. Lee, M. Park, H. Lim, and H. G. Lee, "Magnetization loss and shield effect in multi-stacked tapes with various stacking configurations," *IEEE Trans. Appl. Supercond.*, vol. 16, no. 2, pp. 131–134, Jun. 2006.
[5] S. Celebi, F. Inanir, and M. A. R. LeBlanch, "Coexistence of critical state magnetostriction in type II superconductors: A model exploration," *J. Appl. Phys.*, vol. 101, no. 1, Jan. 2007, Art. no. 013906.
[6] F. Inanir, "Role of superconductivity and paramagnetism in magnetostriction of high-T_c superconductors," *J. Low. Temp. Phys.*, vol. 152, no. 1/2, pp. 63–70, Apr. 2008.
[7] I. Latka, T. Habisreuther, and D. Litzkendorf, "Fiber glass based spatially resolved characterization of flux pinning induced strain of rectangular-shaped bulk YBCO samples," *Phys. C, Supercond.*, vol. 471, no. 11/12, pp. 357–362, Jun. 2011.
[8] H. Yong, Z. Jing, and Y. Zhou, "Magnetostriction and magnetization in deformable superconductors," *Phys. C, Supercond.*, vol. 483, pp. 51–54, Dec. 2012.
[9] H. Ikuta, N. Hirota, Y. Nakayama, K. Kishio, and K. Kitazawa, "Giant magnetostriction in $Bi_2Sr_2CaCu_2O_8$ single crystal in the superconducting state and its mechanism," *Phys. Rev. Lett.*, vol. 70, no. 14, pp. 2166–2169, May 1993.
[10] T. H. Johansen, "Flux-pinning induced stress and strain in superconductor: Long rectangular slab," *Phys. Rev. B, Condens. Matter Mater. Phys.*, vol. 59, no. 17, pp. 11 187–11 190, May 1999.
[11] T. H. Johansen, "Flux-pinning induced stress and strain in superconductor: Case of a long circular cylinder," *Phys. Rev. B, Condens. Matter Mater. Phys.*, vol. 60, no. 13, pp. 9690–9703, Oct. 1999.
[12] T. H. Johansen and D. V. Shantsev, "Magnetostrictive behavior of thin superconducting disks," *Supercond. Sci. Technol.*, vol. 16, no. 9, pp. 1109–1114, Sep. 2003.
[13] W. Feng, X. Han, and P. Ma, "Flux-pinning-induced stress and magnetostriction in functionally graded long rectangular superconductor slab," *J. Appl. Phys.*, vol. 110, no. 6, Sep. 2011, Art. no. 063917.
[14] S. Celebi, F. Inanir, and M. A. R. LeBlanc, "Contribution of the Meissner current to the magnetostriction in a high T_c superconductor," *Supercond. Sci. Technol.*, vol. 18, no. 1, pp. 14–17, Jan. 2005.
[15] F. Inanir, S. Celebi, M. Altunbaş, M. Okutan, and M. Erdogan, "Critical state magnetostriction of type II superconductors under viscous flux flow," *Phys. C, Supercond.*, vol. 459, no. 1/2, pp. 11–17, Aug. 2007.
[16] F. Inanir and S. Celebi, "Model calculations for high-field peak of the fish-tail effect in the magnetostriction of type-II superconductors," *J. Alloys Compd.*, vol. 427, no. 1/2, pp. 1–4, Jan. 2007.
[17] F. Xue, H. Yong, and Y. Zhou, "Effect of flux creep and viscous flux flow on flux-pinning-induced stress and magnetostriction in a long rectangular slab superconductor," *J. Appl. Phys.*, vol. 108, no. 10, Nov. 2010, Art. no. 103910.
[18] Y. H. Zhou and H. D. Yong, "Crack problem for a long rectangular slab of superconductor under an electromagnetic force," *Phys. Rev. B, Condens. Matter Mater. Phys.*, vol. 76, no. 9, Sep. 2007, Art. no. 094523.
[19] J. Zeng, Y. H. Zhou, and H. D. Yong, "Fracture behaviors induced by electromagnetic force in a long cylindrical superconductor," *J. Appl. Phys.*, vol. 108, no. 3, Aug. 2010, Art. no. 033901.
[20] R. G. Mints and E. H. Brandt, "Buckling instability in type-II superconductors with strong pinning," *Phys. Rev. B, Condens. Matter Mater. Phys.*, vol. 61, no. 17, pp. 11 700–11 703, May 2000.
[21] Z. W. Gao, Y. H. Zhou, and K. Y. Lee, "The interaction of two collinear cracks in a rectangular superconductor slab under an electromagnetic force," *Phys. C, Supercond.*, vol. 470, no. 15/16, pp. 654–658, Aug. 2010.
[22] F. Inanir and M. Erdogan, "Effect of transport current on the pinning induced magnetostriction of type-II superconductors," *Acta Phys. Polonica A*, vol. 113, no. 2, pp. 741–752, Feb. 2008.
[23] H. Yong and Y. Zhou, "Stress distribution in flat superconducting strip with transport current," *J. Appl. Phys.*, vol. 109, no. 7, Apr. 2011, Art. no. 073902.
[24] Z. Jing, H. Yong, and Y. Zhou, "Flux-pinning induced interfacial shearing and transverse normal stress in superconducting coated conductor long strip," *J. Appl. Phys.*, vol. 112, no. 4, Aug. 2012, Art. no. 043908.
[25] J. Rhyner, "Vector potential theory of AC losses in superconductors," *Phys. C, Supercond.*, vol. 377, no. 1/2, pp. 56–66, Aug. 2002.
[26] S. Fukui *et al.*, "Numerical analysis of relation between AC loss characteristics and geometrical parameters of multi-layer polygonal conductor assembled by HTS coated conductor," *IEEE Trans. Appl. Supercond.*, vol. 20, no. 3, pp. 2138–2141, Jun. 2010.
[27] F. Gömöry, M. Vojenciak, E. Pardo, and J. Souc, "Magnetic flux penetration and AC loss in a composite superconducting wire with ferromagnetic parts," *Supercond. Sci. Technol.*, vol. 22, no. 3, Mar. 2009, Art. no. 034017.
[28] F. Gömöry and F. Inanir, "AC losses in coil wound from round wire coated by a superconducting layer," *IEEE Appl. Supercond.*, vol. 22, no. 3, Jun. 2012, Art. no. 4704704.
[29] B. Erdem Alaca, M. T. A. Saif, and H. Sehitoglu, "On the interface debond at the edge of a thin film on a thick substrate," *Acta Mater.*, vol. 50, no. 5, pp. 1197–1209, Mar. 2002.

Muzaffer Erdogan was born in Istanbul, Turkey, in 1967. He received the B.S. degree in physics from Istanbul University, Istanbul, Turkey, in 1991, and the M.S. and Ph.D. degrees from Istanbul Technical University, Istanbul, in 1997 and 2008, respectively.

He was as a Research Assistant with the Department of Physics, Istanbul Technical University, until 2009. He is currently an Assistant Professor with Namik Kemal University, Tekirdag, Turkey. He numerically and experimentally studied the properties of the ferromagnetic amorphous wires during his Ph.D. training. His research interests include ac loss reduction in electromagnetic systems such as high-temperature superconductor power transmission cables, as well as the properties of the magnetic nanodot arrays.

Şükrü Yildiz was born in Tokat, Turkey, in 1977. He received the M.S. and the Ph.D. in physics from Gaziosmanpaşa University, Tokat, Turkey, in 2006 and 2011, respectively.

From 2004 to 2013, he was a Research Assistant with the Department of Physics, Gaziosmanpaşa University. Since 2013, he has been an Assistant Professor with the Department of Metallurgical and Materials Engineering, Ahi Evran University, Kirşehir. His research interests include the theoretical performance research of newly designed superconducting microwave device and cable, levitation force measurement, and modeling of superconductors.

Ahmet Cicek received the B.S. degree in physics from, Bilkent University, Ankara, Turkey, in 2003, and the M.S. and Ph.D. degrees in physics from the Institute of Science in Akdeniz University, Antalya, in 2006 and 2012, respectively.

From 2005 to 2010, he was a Research Assistant with Akdeniz University. Afterward, between 2010 and 2014, he was a Research Assistant with the Department of Physics, Mehmet Akif Ersoy University, Burdur, Turkey, where he has been a Faculty Member since 2014. He is currently a Postdoctoral Scholar with the Department of Electrical Engineering, Jack Baskin School of Engineering, University of California at Santa Cruz, Santa Cruz, CA, USA. He studied numerical investigations of Kerr nonlinear photonic crystals and density functional theoretical investigations of graphene–substrate interactions during his M.S. and Ph.D. studies, respectively. His research interests include numerical and experimental investigation of high-T_c superconductors, all-optical and all-acoustic photonic- and phononic-crystal-based devices, nanoplasmonic devices, and microfluidics.

Fedai Inanir was born in Samsun, Turkey, in 1976. He received the B.S. degree in physics from Mayis University, Samsun, Turkey, in 1997 and the M.S. and Ph.D. degrees from the Karadeniz Technical University, Trabzon, in 2002 and 2006, respectively.

He joined the Department of Physics, Rize University (later changed to Recep Tayyip Erdoğan University), Rize, Turkey, where he was a Research Assistant until 2006, and then an Assistant Professor until 2009. He is currently a Professor with Yildiz Technical University, Istanbul, Turkey. He studied numerical investigations of magnetomechanical interaction of superconducting materials and devices during Ph.D. training. His research interests include electromagnetic design of high-T_c superconductor devices, such as superconducting power wires and superconducting generators, and MRI magnet design.